2011 IEEE International Conference on Rehabilitation Robotics
Rehab Week Zurich, ETH Zurich Science City, Switzerland, June 29 - July 1, 2011

# Multijoint arm stiffness during movements following stroke: implications for robot therapy

D. Piovesan, M.Casadio, F. A. Mussa-Ivaldi
Sensory Motor Performance Program
Rehab. Institute of Chicago/Northwestern University
Chicago, Illinois, USA
d-piovesan@northwestern.edu

P.G Morasso
Dept. of Communication Computer and System Science,
University of Genova
Italian Institute of Technology
Genova, Italy

*Abstract*— **Impaired arm movements in stroke appear as a set of stereotypical kinematic patterns, characterized by abnormal joint coupling, which have a direct consequence on arm mechanics and can be quantified by the net arm stiffness at the hand. The current available measures of arm stiffness during functional tasks have limited clinical use, since they require several repetitions of the same test movement in many directions. Such procedure is difficult to obtain in stroke survivors who have lower fatigue threshold and increased variability compared to unimpaired individuals. The present study proposes a novel, fast quantitative measure of arm stiffness during movements by means of a Time-Frequency technique and the use of a reassigned spectrogram, applied on a trial-by-trial basis with a single perturbation. We tested the technique feasibility during robot mediated therapy, where a robot helped stroke survivors to regain arm mobility by providing assistive forces during a hitting task to 13 targets covering the entire reachable workspace. The endpoint stiffness of the paretic arm was estimated at the end of each hitting movements by suddenly switching of the assistive forces and observing the ensuing recoil movements. In addition, we considered how assistive forces influence stiffness. This method will provide therapists with improved tools to target the treatment to the individual's specific impairment and to verify the effects of the proposed exercises.**

***Keywords- stiffness, arm impedance, stroke, robot therapy***

## I. INTRODUCTION

Recovery of arm function is a crucial goals following stroke and restoring intra-limb coordination remains an important goal in physical therapy [1]. Treatment strategies generally focus on sensorimotor intervention (e.g., constraint-induced movement therapy)[2, 3], progressive-resistive [4], and robot mediated training [5-7] with emphasis on maximizing functional use of the impaired limb.

A well-known consequence of stroke is the appearance of stereotypical and anomalous kinematic patterns due to abnormal synergistic muscle activations. Even though these abnormal synergies have been extensively studied [8-10], our understanding of the physiological and biomechanical characteristics of the phenomenon still remains limited. Abnormal muscle activations have direct and indirect consequences on limb mechanics, including modified tixotropic characteristics of connective tissues, and the overall effect on movement is quantifiable by the net mechanical impedance. Previous experiments aiming at quantifying limb impedance in stroke survivors focused on postural and single joint movements [11, 12]. An attempt was made to measure stiffness during multijoint passive movements [13]; however, greater insight on the physiological consequence of abnormal muscles' activations can be gained from the analysis of more complex tasks such as reaching or hitting. Current methods to measure impedance during movements are based on regression techniques [14, 15]. These methods have limited clinical use since they require several repetitions of the same kind of movement, which are difficult to obtain in stroke survivors.

The objective of this study is to examine the mechanisms of abnormal arm impedance regulation during movements by means of a new technique which requires a single brief perturbation during a single movement rather than the repetition of multiple trials perturbed in different directions [16]. Although frequency domain methods have previously been used to estimate stiffness and damping [17], the method presented here allows the estimation of such variables as a function of time. Thus, local limb stability can be assessed during movements. The knowledge of local stability has major functional implications since it identifies how a subject can interact with the environment as well as the compensation strategies to stabilize the system used by each individual.

This study tested the possibility to use the proposed technique during robot mediated therapy for obtaining valuable physiological and biomechanical information on the behavior of stroke survivors during training. We assessed the influence of different aiding forces on the estimation of arm stiffness demonstrating that this quantitative measure is instrumental to assess differences in limb mechanics among individuals with different levels of impairments. This would help therapists to prescribe and assess treatments on a case-by-case basis.

## II. METHODS

We estimated the endpoint stiffness of stroke survivors' paretic arm during robot mediated therapy trials by means of a Time-Frequency domain identification technique. The experimental training protocol has been previously reported [6] and is summarized here for clarity. Subjects were trained using a hitting task over a large workspace, while a robot provided an aiding force. This force, was aimed at the target, and remained constant until the target was reached, where it was suddenly turned off.. We used this sudden drop of force as a convenient perturbation to be used in the estimation of arm stiffness [18] because it did not interfere with the ongoing training procedure

TABLE I SUBJECT CHARACTERISTICS

| | Age | DD | FM before | FM after | FM 3 m a | Ash | Gender | E | PH |
|---|---|---|---|---|---|---|---|---|---|
| **S1** | 72 | 28 | 6 | 8 | 7 | 3 | M | I | L |
| **S2** | 69 | 25 | 12 | 18 | 22 | 1+ | F | I | R |
| **S3** | 57 | 40 | 17 | 21 | 18 | 3 | M | I | L |
| **S4** | 34 | 24 | 13 | 23 | 24 | 1+ | F | I | R |
| **S5** | 30 | 12 | 6 | 9 | 11 | 2 | F | I | L |
| **S6** | 46 | 26 | 6 | 13 | 16 | 2 | F | H | L |
| **S7** | 55 | 76 | 36 | 41 | 41 | 1 | F | H | L |
| **S8** | 59 | 39 | 5 | 8 | 7 | 3 | F | I | R |
| **S9** | 53 | 39 | 41 | 45 | 42 | 1 | F | H | R |

Subjects data. Age: years. DD= duration of disease (months) FM = upper arm Fugl- Meyer score, max 66/66; before, after and after three months with respect to the robot therapy sessions, Ash= Ashworth score, Gender: M=male, F=female; E= Etiology: I=ischemic, H= Hemorrhagic; PH=paretic hand: L=Left, R=Right

and passed largely un-noticed by the patient. However, the technique can be applied to a large variety of perturbations.

### A. *Subjects*

Nine chronic stroke survivors (1-12 years post stroke) participated in the study after signing informed consent conform to the ethical standards of the Helsinki declaration. The characteristics of the subjects are described in Tab. I

### B. *Task*

Subjects sat in a chair while grasping the handle of the manipulandum "Braccio di Ferro"[19]. A custom built cast restrained the movement of the wrist. A light support was connected to the forearm to allow low-friction sliding on the horizontal surface of a table (fig.1). The translation of the shoulder was eliminated using a harness connected to the chair. The arm motion was restricted to the horizontal plane, eliminating the influence of gravity; hence, only shoulder and elbow flexion/extension were allowed and their motion was assisted according to equation 1.Endpoint position was collected at 1 kHz using the robot encoders. The visual representation of the targets was obtained with a 19" screen positioned vertically in front of the subject at a distance of about 1 m. A set of round targets (diameter 2 cm) were located

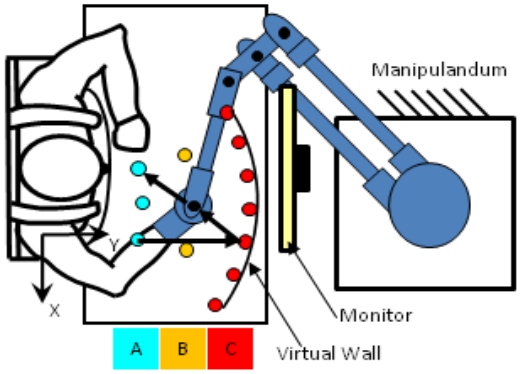


Figure 1. Experimental Setup

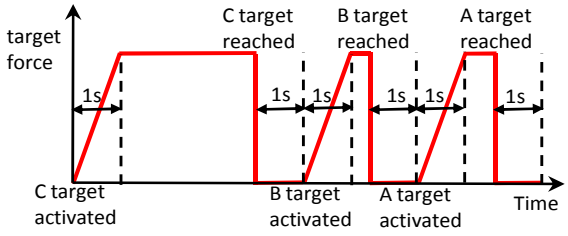


Figure 2. Force Field, Structure of the basic trial.

on three concentric circles centred at the shoulder, as depicted in fig. 1. The difference in radius between each circumference was 10 cm; within each circle the targets were by distances of 6.26cm (A), 8.77 cm (B),and 5.65 cm (C).

A stereotypical trial is described by the following steps:

1. From one of the three starting positions 'A' one of the seven 'C' targets was randomly selected (fig.1); the aiding force was turned on; an acoustic feedback was given synchronously with the reaching of the target while the aiding force was suddenly turned off for a time interval of 1s (fig. 2);
2. Point 1 was repeated for the 'C' to 'B' transition after having randomly selected the 'B' target;
3. Point 2 was repeated for the 'B' to 'A' transition after having randomly selected the 'A' target.

The duration of the wait and rise times for each trajectory within the trial was 1 s (fig. 2). The aforementioned three steps were repeated so to have three presentations of each of the seven 'C' targets for a total of sixty-three movements (3x3x7). The overall protocol consisted of four blocks of trials. The therapist could decide, in accordance with the subject, to extend the session with additional blocks characterized by lower levels of force. The overall duration of the sessions ranged from 45 to 75 minutes.

### C. *Force fields*

The haptic representation of the targets was generated by the robot according to the following impedance control equation:

$$T_m = J^T \left\{ \rho(F) \frac{(x_T - x_H)}{|x_T - x_H|} + \begin{bmatrix} B_r & 0 \\ 0 & B_r \end{bmatrix} \dot{x}_H + F_w(x_H, x_w, K_w) \right\} \quad (1)$$

where $x_T$ is the target position, $x_H$ is the position of the hand/handle, $F$ is the maximum level of the force field (see Tab. II), $\rho(F)$ is the activation function of the field (a ramp with a rise time of 1s), and $J$ is the Jacobian matrix of the robot arm, whose transpose matrix maps the desired force to be transmitted by the handle into the torque that must be delivered by the motors. The two additional terms in Eq.1 represent a viscous field to stabilize the arm posture and a rigid wall beyond the circle of 'C' targets, which provided a haptic representation of the boundary of the workspace. The viscous

TABLE II MINIMUM AIDING FORCE FOR EACH SESSION

| | Max Force | Session | | | | | | | | | |
|---|---|---|---|---|---|---|---|---|---|---|---|
| | | **1** | **2** | **3** | **4** | **5** | **6** | **7** | **8** | **9** | **10** |
| **S1** | 25 | 25 | 18 | 18 | 15 | 15 | 15 | 15 | 13 | 13 | 10 |
| **S2** | 15 | 13 | 12 | 12 | 10 | 9 | 9 | 6 | 6 | 6 | 6 |
| **S3** | 13 | 10 | 10 | 9 | 8 | 8 | 8 | 7 | 6 | 5 | 4 |
| **S4** | 9 | 6 | 6 | 6 | 5 | 5 | 7 | 5 | 4 | 2 | 2 |
| **S5** | 9 | 5 | 4 | 3 | 3 | 3 | 3 | 3 | 3 | 3 | 2 |
| **S6** | 13 | 8 | 8 | 8 | 7 | 7 | 9 | 6 | 5 | 4 | 4 |
| **S7** | 5 | 2 | 1 | 0 | 0 | 0 | 0 | 0 | 0 | 0 | 0 |
| **S8** | 22 | 20 | 18 | 16 | 16 | 14 | 12 | 12 | 12 | 12 | 8 |
| **S9** | 5 | 3 | 2 | 1 | 0 | 0 | 0 | 0 | 0 | 0 | 0 |

Minimum level of aiding force reached for each subject at different sessions. Each session started with the maximum level of force (gray column). Hence, an intra-subject comparison of stiffness with the same aiding force was possible between the first and the last session. The force range of 5-6N encompassed the majority of subjects, and was used to assess the relationship between estimated stiffness and Ashworth score. We performed a sensitivity analysis between force and stiffness at 5, 10, and 15N.

coefficient $B_r$ was empirically determined to be 12Ns/m as a trade-off between stability and dissipated energy, while the stiff virtual wall was rendered with a 1000 N/m elastic coefficient $K_w$.

The force level of the robot facilitation was selected by the physical therapist as the minimum value that evoked a functional response, i.e. a movement in the intended direction. The initial assistive force is subject-specific, and might depend upon the reachable space that each subject can achieve in the workspace, which the Fugl-Meyer [20] and modified Ashworth [21] scores cannot always describe. The minimum assistive force chosen in the first session was always presented to the subject in the following sessions. This allowed us to evaluate throughout the treatment the improvement of arm kinematics. As the therapy proceeded, lower levels of force were applied to comply with the improvement of the subject. The minimum force applied in each session is presented in Tab. II.

### *D. Time Frequency Domain*

The sudden drop of the assistive force towards the end of a trial can be considered as a "hold & release" type of perturbation [18]. Hence, the residual vibration of the arm in the Cartesian space $\overrightarrow{\partial X} = (x, y)$ can be monitored. By tracking the vibrational frequency as a function of time, stiffness and damping can be calculated using mathematical tools from modal analysis.

To estimate the impedance parameters of the arm from the "hold & release" response, we assumed that the arm behaved as a second order system, following the equation:

$$I(X,t)\overrightarrow{\partial\ddot{X}}(t)+B(\dot{X},X,t)\overrightarrow{\partial\dot{X}}(t)+K(\ddot{X},\dot{X},X,t)\overrightarrow{\partial X}(t)=0 \quad (2)$$

where $I$, $B$, and $K$ are the matrices of inertia, damping and stiffness, respectively. The use of higher order models might have given further insight on the reflexive nature of the system; however, a numerical optimization dependent on the assumption of a cost function would have been required.

Assuming that the recorded response is a solution of equation 2, the identification of the system resonant angular frequencies $\omega_i$ can be carried out using a set of generic elementary functions $g(t)$, commonly called "windows". The main feature of a window function is to be simultaneously localized both in the time and frequency domains. If we think of the window $g(t)$ sliding along the non-stationary time-variant signal $x(t)$, for each time shift $\tau$ we can compute the Fourier transform of the product $x(t)\cdot g(t-\tau)$. Such function is called "Short Term Fourier Transform" (STFT) and can be expressed as:

$$STFT(\omega,\tau)=\int_{-\infty}^{+\infty} x(t)\cdot g(t-\tau)e^{-j\omega t}dt \quad (3)$$

A spectrogram is a representation of the STFTs magnitude calculated on the signal $x(t)$ for multiple time shifts $\tau$. The spectrum of the signal at one instant is calculated as the average of all STFTs enclosing that instant in the time window and the magnitude peaks identify the resonant frequencies of the system. However, the intrinsic algorithm necessary to calculate the spectrogram "smears" the energy density in the neighborhood of time and frequency, due to the extensive averaging of all the windows encompassing a certain instant. Thus, it is difficult to precisely identify the resonant frequencies by only looking at the peaks of $STFT(\omega,\tau)$ magnitude. To overcome this drawback, a method known as reassigned spectrogram (RS) was used to track the variation of instantaneous frequencies after the perturbation [22].

From complex analysis, a maximum of $STFT(\omega,\tau)$ can be computed by identifying where the phase of the complex function reaches a steady state [22]. Thus, by calculating the partial derivatives of STFT phase, with respect to time and frequency, allows us to identify where the stationary phase is with respect to the location of the window in time and frequency, identifying a time delay and frequency shift that can be used to "reassign' the position of maximum energy [23]. To calculate the STFT spectrogram, we used a 0.75s Kaiser window, with β=3, convolving the window every 2ms. The same parameters were used to calculate the reassigned spectrogram. When the instantaneous frequencies were identified in the RS, we used a Savitzky-Golay polynomial filter [24] to obtain a continuous time-varying frequency function.

### *E. Eigenvalues*

Given the duality between time and frequency domain, the matrix coefficients of (2) can be estimated by monitoring the natural frequencies and vibrational modes of the system [25]. To solve such problem, equation 2 must be decoupled in a set of mutually independent equations whose coefficients are functions of the time-varying resonant frequencies of the

system. To this purpose, (2) ought to be normalized to a monic system, where spectral algebraic theory easily applies [26].

We first estimated the inertial parameters of the subjects' arm with respect to the shoulder and elbow joints using a regressive equation [27]. Hence, the endpoint inertial matrix was calculated by means of the Jacobian operator of the subject's arm between the joint space and the Cartesian space [28]. Since the inertial matrix is real and positive definite, it admits real squared roots. Without loss of theoretical rigor, we could consider only the positive square roots of the inertial matrix, which generates a new positive definite matrix that admits inverse. Thus, matrix $I^{-\frac{1}{2}}$ exists and is symmetric and real. This matrix is used to normalize (2) into a new monic system, whose eigenvalues are the same of (2) [25], namely.

$$\ddot{\vec{\partial Y}}(t)+\tilde{B}\dot{\vec{Y}}(t)+\tilde{K}\vec{Y}(t)=0 \tag{4}$$

where

$$I^{-\frac{1}{2}}\cdot I\cdot I^{-\frac{1}{2}}=\delta_{ij};\;\; I^{-\frac{1}{2}}\cdot B\cdot I^{-\frac{1}{2}}=\tilde{B};\; I^{-\frac{1}{2}}\cdot K\cdot I^{-\frac{1}{2}}=\tilde{K}$$
$$\vec{Y}=I^{\frac{1}{2}}\cdot\vec{\partial X} \tag{5}$$

The decoupling of (4), can be obtained by pre- and post-multiplying each matrix of (5) by the eigenvector matrix $P$ of $\tilde{K}$ which represents the directions of the vibrational modes in the Cartesian space, namely:

$$\ddot{\vec{\partial Y}}(t)+diag[2\Gamma]\dot{\vec{Y}}(t)+diag[\eta^2]\vec{Y}(t)=0 \tag{6}$$

In general, the normalized resonant frequency $\eta^2(t)$ and normalized damping factor $\Gamma(t)$ are time-varying and can be estimated as follows [29]:

$$\Gamma(t)=-\sigma-\frac{\dot{\omega}_i}{2\omega_i};\;\; \eta^2(t)=\omega_i^2+\sigma^2+\frac{\sigma\dot{\omega}_i}{\omega_i}-\dot{\sigma} \tag{7}$$

where

$$\sigma(t)=\frac{d}{dt}\ln A(t)=\frac{\dot{A}(t)}{A(t)} \tag{8}$$

Therefore, by obtaining the instantaneous amplitude $A(t)$ and the instantaneous resonant angular frequency $\omega_i(t)$ from the RS (fig.3), and the eigenvector matrix $P$ it is possible to reconstruct $B$ and $K$ using equations (4-8).

### F. *Eigenvectors*

To obtain a real matrix ( $P\in\Re$ ), the system ought to be classically damped. It follows that the eigenvectors of the damping matrix $\tilde{B}$ are aligned with those of the stiffness matrix $\tilde{K}$, and that the vibrational modes of the system have fixed nodes in the chosen reference frame [30].

From linear algebra, the general solution of (2) is the linear combination of all the solutions of the eigenproblem:

$$\vec{\partial X}=\sum_{j=1}^{n}a_j\vec{v}_j e^{\lambda_j t}+b_j\bar{\vec{v}}_j e^{\bar{\lambda}_j t}=\sum_{j=1}^{n}\vec{s}_j \tag{9}$$

where $\vec{p}_j=\vec{v}_j=\bar{\vec{v}}_j$ are the eigenvectors (i.e. the directions of the vibrational modes in the Cartesian space) of matrix $\tilde{K}$. In our case, since the system has 2 planar degrees of freedom, the solution is also equal to the super-position of each damped mode of vibration $\vec{s}_j$.

$$\vec{\partial X}=\vec{s}_1+\vec{s}_2=\begin{Bmatrix}s_{1_1}\\ s_{1_2}\end{Bmatrix}+\begin{Bmatrix}s_{2_1}\\ s_{2_2}\end{Bmatrix}=$$
$$=C_1e^{\alpha_1 t}\cos(\omega_1 t-\psi_1)\begin{Bmatrix}p_{1_1}\\ p_{1_2}\end{Bmatrix}+C_2e^{\alpha_2 t}\cos(\omega_2 t-\psi_2)\begin{Bmatrix}p_{2_1}\\ p_{2_2}\end{Bmatrix} \tag{10}$$

The modes can then be identified by means of a filtering process and, since $\vec{p}_1$ and $\vec{p}_2$ are mutually orthogonal, using a single value decomposition (SVD) between $s_{1_1}$ and $s_{1_2}$ identifies respectively $\vec{p}_1$ and its orthogonal $\vec{p}_2$.

## III. RESULTS

### A. *Stiffness tracking*

A stereotypical response to the perturbation is depicted in figure 3a. The stiffness and damping can be estimated by means of the frequency tracks and amplitude decay of the STFT spectrogram (fig.3b). The STFT and its reassignment (fig 3c) have the same amount of points. However, the points that were "smeared" in the neighborhood of the STFT peaks are concentrated on a narrower bandwidth in the RS. This re-mapping algorithm can provide a "super-resolution" in both time and frequency compared to STFT. However, the super-resolution cannot be constant throughout the frequency and time domain, because of its dependency on the smearing of the energy caused by the convolving windows.

Arm stiffness can be influenced by three separate factors: the intrinsic stiffness of muscles and tendons, the level of

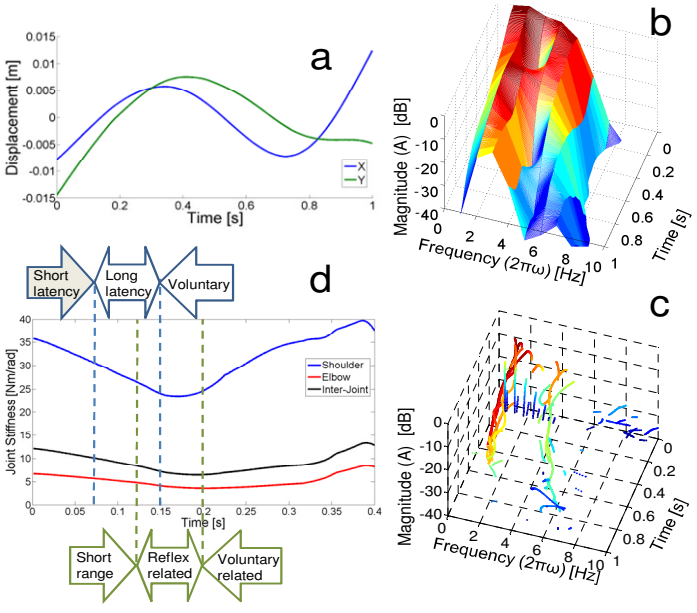


Figure 3. a) Exemple of oscillation after negative force step. b) STFT, c) Reassigned Spectrograms, and d) time-varing stiffness, Subject S7, Force 5N, central target of circle B in Fig.1, last session.

voluntary co-contraction, and the intervention of reflexes of various natures. The technique that we propose cannot separate the estimations of these three components as other methods can do [31]. However, we can observe the influences of each factor as the estimated stiffness changes in time (fig 3d): the intrinsic stiffness is mostly dependent upon the biomechanics of the limb and it influences the stiffness estimation right after the perturbation is applied; stretch sensitive reflexes, act usually on a specific time scale, between 70 and 150ms after the perturbations onset, and their effect is visible on the stiffness estimation with 50ms delay [32, 33]. To highlight the reflexes' contribution to the stiffness, all the estimations and relative statistics were calculated at 200ms after the perturbation onset. Later estimates are influenced by voluntary control, among other factors.

### *B. Stiffness and Damping variation through the workspace*

Figure 4 presents a stereotypical distribution of stiffness and damping ellipses for subject S2, where the stiffness was tested using 3 different levels of force (i.e. 5-10-15N) at 200ms after the perturbation. We can notice that the shape of the ellipses is quite repeatable within the workspace, even though the magnitude depends upon the force level and the position. Most remarkably, a higher force will elicit a higher stiffness in a position of the workspace that is more difficult to reach for the subject. This is immediately noticeable by examining the velocity profiles to reach the target. The shape of the ellipses is mostly elongated in the direction where the aiding force was acting before hitting the target. We can notice that the magnitude of damping is about 1 order of magnitude smaller compared to stiffness. Since there are no well-known neural mechanisms for the modulation of damping, in this work we will focus on the modulation of stiffness.

### *C. Effect of treatment on Stiffness*

We calculated the variation of the average stiffness of the workspace between the first and last session of each subject. Each individual started with the minimal assistive force required to initiate the movement, and each following session started with such values. We chose two metrics for the comparison: the average of the stiffness matrix determinant and the average of the maximum eigenvalues throughout the workspace (fig.5). Both metrics decreased during traning, indicating the beneficial effect of the therapy in diminishing hypertonic activity/spasticity and increasing the ability to regulate the interaction with the environment.

Levels of stiffness metrics are higher in the first session for subjects with lower Ashworth score (Ash); however, such subjects are also those who have greater percent decrease in stiffness at the end of therapy. Metrics populations were compared using a one-way ANOVA whose result are reported in Table III (level of significance p=0.05). For most of the subjects with higher Ashworth score, even though a decrease in stiffness was found, it was not statistically significant. However, a repeated measured ANOVA, with subject as a random factor confirmed a statistical decrease in stiffness metrics after the rehabilitation process.

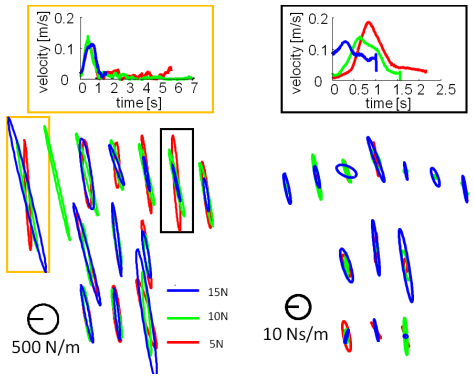


Figure 4. Stiffness and damping estimations for S2 (Ash. 1+) for each target of the workspace, with 3 levels of aiding force. On top, velocity profiles to reach two targets (yellow and black squares, respectively)

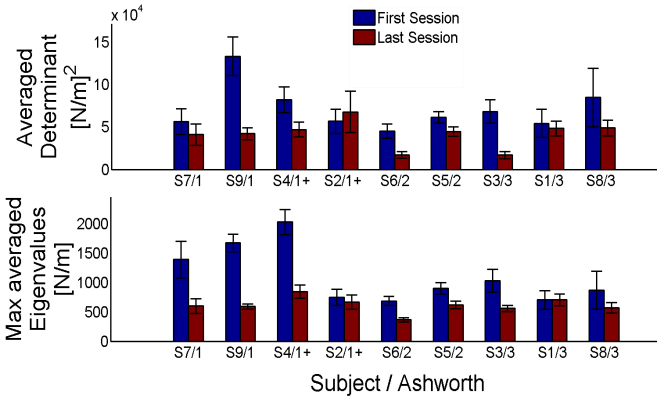


Figure 5 Comparison between the stiffness metrics between the first and the last session using the same level of force. Force level was chosen as the minimal to initiate the movement. For significant statistical differences in the metrics populations see Table III.

### *D. Stiffness as a function of Ashworth Score*

Although a statistically significant decrease of the stiffness metrics were detected, as a consequence of the training (Tab. I), they were not associated with changes of the Ashworth score. To address the relationship between the Ashworth score and a global measure of stiffness, we again considered the average of the stiffness matrices' determinants throughout the workspace. For a fair comparison, we considered a set of sessions towards the end of the training where the majority of subjects could reach similar aiding forces. We computed the average determinant of the last 3 sessions with maximal aiding force ranging from 5 to 6 N. The relationship between the Ashworth score and the average determinant is reported in fig.6.

A series of one-way ANOVAs were computed to verify any significant difference in the populations of chosen stiffness metrics calculated for different Ashworth score groups. We found no significant difference within each Ashworth group. Moreover, no significant difference was found between the group with Ash=1 and Ash=1+ (F=0.4, p=0.54). However, significant difference was found when comparing Ash=1,1+ with Ash=2 (F=5,27, p=0.018) and Ash=2 with Ash=3 (F=15.11, p=0.006).

TABLE III STIFFNESS STATISTICAL COMPARISON BETWEEN THE FIRST AND LAST SESSION

| | Max Force[N] | Ash | Determinant | | Max Avg. Eigenvalue | |
|---|---|---|---|---|---|---|
| | | | F(1,24) | p | F(1,24) | p |
| **S7** | 5 | 1 | 0.73 | 0.400 | 6.61 | 0.017 |
| **S9** | 5 | 1 | 17.24 | <0.0001 | 56.17 | <0.0001 |
| **S4** | 12 | 1+ | 4.77 | 0.039 | 28.96 | <0.0001 |
| **S2** | 15 | 1+ | 0.18 | 0.678 | 0.23 | 0.634 |
| **S6** | 9 | 2 | 11.16 | 0.003 | 16.12 | <0.0001 |
| **S5** | 9 | 2 | 4.45 | 0.046 | 7.08 | 0.014 |
| **S3** | 12 | 3 | 15.14 | <0.0001 | 6.44 | 0.018 |
| **S1** | 25 | 3 | 0.12 | 0.728 | <0.0001 | >0.9999 |
| **S8** | 22 | 3 | 1.2 | 0.240 | 0.96 | 0.338 |
| | | | **F (1,8)** | **p** | **F (1,8)** | **p** |
| **Repeated Measures** | | | 9.39 | 0.015 | 12.59 | 0.007 |

Statistical significance of the metrics used to represent stiffness globally.

## IV. DISCUSSION AND CONCLUSION

We demonstrated how stiffness can be best characterized as a "local" variable that is a function of time, limb kinematics in the workspace, assistive force, and level of impairment of the subject. Our measures indicated that when all of the above conditions are within a certain tolerance, the proposed estimating method is fairly repeatable. The technique can effortlessly be implemented during robot therapy and allows for an online checking of the subject rehabilitation process. Even though mechanical external vibration could compromise the measuring process the vibrational modes of the robot are generally at higher frequency compared to those monitored for the stiffness estimation, and can be easily rejected. On the other hand, this requires to previously measure the resonant frequencies of the robot off-load.

In Sec. III.C we observed that at the beginning of training, stiffness metrics estimated on subjects with Ash=1/1+ were higher compared to the metrics estimated for subject with greater Ashworth score. This result seems to contradict the notion that the Ashworth score is a representation of stiffness. Moreover, we observed that in the direction of higher impairment stiffness increased as the aiding force increased (as we described in Sec. III.B). Hence, we would have expected to find lower stiffness for people with lower Ashworth score, also because they started the training with a lower level of force. Conversely, at the end of training we found that subjects with lower Ashworth score greatly diminished their stiffness, while individual with higher Ashworth score did not. Likewise, we expected to find a decrease of Ashworth score for subjects that had a considerable decrease in stiffness with training, but such changes were not found. We hypothesize that at the beginning of the training the higher stiffness estimated in individuals with lower Ashworth score is due to the reflexive component of the stiffness, while for subjects with high Ashworth score, such component is limited as demonstrated in [31]. Since the subjects participated to a similar training process the influence of soft tissue contractures would be similar among them. Thus, the decrease in stiffness observed in subjects with

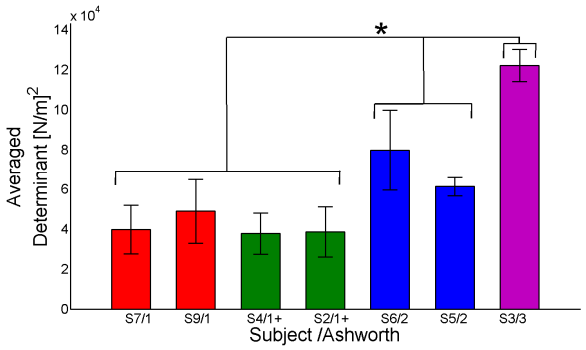


Figure 6. Relarionship between Ashworth score and the determinants of the stiffness matrices averaged throughout the workspace. * indicates groups that are statistically different.

lower Ashworth score might depend upon an improved reflexes modulation. We suggest that the Ashworth score is keener to represent the rigidity of the connective and muscular (active) tissue [11], not the reflexive component of spasticity [31]. While stiffness has been long considered an index for spasticity/tonicity, we suggest that when associated to its hand-position dependency in the workspace it can be an appropriate quantitative measure of functionality. Indeed, while the Fugl-Meyer score indicates the possible configuration that the limb can assume, and the Ashworth score gives a global evaluation of muscular rigidity, the local stiffness is complementary to these two assessments and helps to identify how mobile the limb is and the specific intervention to improve mobility. Moreover, the shape of the stiffness ellipses indicates if the impairment depends on a specific joint (orientation of the stiffness), is due to general co-contraction (magnitude and roundness of the ellipses), or can be overcome by planning different reaching trajectory. This goes toward a personalized therapy and can help in specific pharmaceutical intervention such as botulinum toxin injections.


## ACKNOWLEDGMENT

This research was supported by NNINDS grant 2R01NS035673 and EU grant HUMOUR (FP7-ICT-231724). Authors would like to thanks Psiche Giannoni for her valuable contribution to this work.


## REFERENCES


[1] S. Brunnstrom, *Movement Therapy in Hemiplegia: A Neuropsychological Approach*. New York: Harper and Row, 1970.

[2] J. Liepert, *et al.*, "Motor cortex plasticity during constraint-induced movement therapy in stroke patients," *Neurosci Lett,* vol. 250, pp. 5-8, 1998.

[3] E. Taub, *et al.*, "A placebo-controlled trial of constraint-induced movement therapy for upper extremity after stroke," *Stroke,* vol. 37, pp. 1045-1049, 2006.

[4] R. W. Bohannon, *et al.*, "Rehabilitation Goals Of Patients With Hemiplegia," *International Journal Of Rehabilitation Research,* vol. 11, pp. 181-183, 1988.

[5] M. Casadio, *et al.*, "Robot therapy of the upper limb in stroke patients: preliminary experiences for the

principle-based use of this technology," *Funct Neurol,* vol. 24, pp. 195-202, Oct-Dec 2009.

[6] M. Casadio*, et al.*, "A proof of concept study for the integration of robot therapy with physiotherapy in the treatment of stroke patients," *Clin Rehabil,* vol. 23, pp. 217-28, Mar 2009.

[7] J. L. Patton*, et al.*, "Evaluation of robotic training forces that either enhance or reduce error in chronic hemiparetic stroke survivors," *Exp Brain Res,* vol. 168, pp. 368-383, Jan 2006.

[8] J. P. Dewald*, et al.*, "Abnormal muscle coactivation patterns during isometric torque generation at the elbow and shoulder in hemiparetic subjects," *Brain,* vol. 118 ( Pt 2), pp. 495-510, 1995.

[9] R. F. Beer*, et al.*, "Deficits in the coordination of multijoint arm movements in patients with hemiparesis: evidence for disturbed control of limb dynamics.," *Experimental Brain Research,* vol. 131, pp. 305-319, 2000.

[10] D. J. Reinkensmeyer*, et al.*, "Directional control of reaching is preserved following mild/moderate stroke and stochastically constrained following severe stroke," *Exp Brain Res,* vol. 143, pp. 525-30, Apr 2002.

[11] E. de Vlugt*, et al.*, "The relation between neuromechanical parameters and Ashworth score in stroke patients," *Journal of NeuroEngineering and Rehabilitation,* vol. 7, p. 35, 2010.

[12] J. J. Palazzolo*, et al.*, "Stochastic estimation of arm mechanical impedance during robotic stroke rehabilitation," *IEEE Trans Neural Syst Rehabil Eng,* vol. 15, pp. 94-103, 2007.

[13] L. Q. Zhang*, et al.*, "Shoulder, elbow and wrist stiffness in passive movement and their independent control in voluntary movement post stroke," in *IEEE 11th international conference on rehabilitation robotics*, Kyoto, Japan, 2009, pp. 805-811.

[14] E. Burdet*, et al.*, "A method for measuring endpoint stiffness during multi-joint arm movements," *Journal of biomechanics,* vol. 33, pp. 1705-1709, 2000.

[15] M. Darainy*, et al.*, "Control of Hand Impedance Under Static Conditions and During Reaching Movement," *J Neurophysiol,* vol. 97, pp. 2676-2685, April 1, 2007 2007.

[16] D. Piovesan*, et al.*, "A new time-frequency approach to estimate single joint upper limb impedance," *Conf Proc IEEE Eng Med Biol Soc,* vol. 2009, pp. 1282-5, 2009.

[17] T. E. Milner and C. Cloutier, "Compensation for mechanically unstable loading in voluntary wrist movement," *Exp Brain Res,* vol. 94, pp. 522-32, 1993.

[18] S. B. Bortolami*, et al.*, "Analysis of human postural responses to recoverable falls," *Exp Brain Res,* vol. 151, pp. 387-404, Aug 2003.

[19] M. Casadio*, et al.*, "Braccio di Ferro: A new haptic workstation for neuromotor rehabilitation," *Technology and Health Care,* vol. 14, pp. 123-142, 2006.

[20] A. R. Fugl-Meyer*, et al.*, "The post-stroke hemiplegic patient. 1. a method for evaluation of physical performance," *Scand J Rehabil Med,* vol. 7, pp. 13-31, 1975.

[21] R. Bohannon and M. Smith, "Interrater reliability of a modified Ashworth scale of muscle spasticity," *Phys Ther,* vol. 67, pp. 206 - 207, 1987.

[22] D. J. Nelson, "Cross-spectral methods for processing speech," *The Journal of the Acoustical Society of America,* vol. 110, pp. 2575-2575, 2001.

[23] F. Auger and P. Flandrin, "Representations by the Reassignment Method," *IEEE TRANSACTIONS ON SIGNAL PROCESSING,* vol. 43, pp. 1068-1089, 1995.

[24] W. H. Press*, et al.*, *Numerical Recipes in C: The Art of Scientific Computing,*, 2nd ed.: Cambridge University Press., 1992.

[25] D. J. Inman, *Vibration: with control, measurement, and stability* vol. 7. Englewood Cliffs, NJ: Prentice Hall, 1989.

[26] P. Lancaster and U. Prells, "Inverse problems for damped vibrating systems," *Journal of Sound and Vibration,* vol. 283, pp. 891-914, 2005.

[27] V. Zatsiorsky and V. Seluyanov, "The mass and inertia characteristics of the main segments of the human body 30," in *International Congress of Biomechanics: Biomechanics VIII-B*, Champaign, Illinois, 1983, pp. 1152-1159.

[28] D. Piovesan*, et al.*, "Comparative analysis of methods for estimating arm segment parameters and joint torques from inverse dynamics," *J Biomech Eng,* vol. 133, p. 031003, Mar 2011.

[29] L. Cohen*, et al.*, "Time-frequency analysis of a variable stiffness model for fault development," *Digital Signal,* vol. 440, pp. 429-440, 2002.

[30] D. J. Ewins, *Modal testing: theory, practice and applications*, Second Edition ed. Baldock,Hertfordshire, England: Research Studies Press LTD., 2000.

[31] L. Alibiglou*, et al.*, "The relation between Ashworth scores and neuromechanical measurements of spasticity following stroke," *Journal of NeuroEngineering and Rehabilitation,* vol. 5, p. 18, 2008.

[32] a. a. Frolov*, et al.*, "On the possibility of linear modelling the human arm neuromuscular apparatus," *Biological cybernetics,* vol. 82, pp. 499-515, 2000.

[33] A. A. Frolov*, et al.*, "Adjustment of the human arm viscoelastic properties to the direction of reaching," *Biological cybernetics,* vol. 94, pp. 97-109, 2006.